

# Convolutional Experts Network for Facial Landmark Detection

Amir Zadeh\*

Carnegie Mellon University  
5000 Forbes Ave, Pittsburgh, PA 15213, USA  
abagherz@cs.cmu.edu

Tadas Baltrušaitis\*

Carnegie Mellon University  
5000 Forbes Ave, Pittsburgh, PA 15213, USA  
tbaltrus@cs.cmu.edu

Louis-Philippe Morency

Carnegie Mellon University  
5000 Forbes Ave, Pittsburgh, PA 15213, USA  
morency@cs.cmu.edu

## Abstract

*Constrained Local Models (CLMs) are a well-established family of methods for facial landmark detection. However, they have recently fallen out of favor to cascaded regression-based approaches. This is in part due to the inability of existing CLM local detectors to model the very complex individual landmark appearance that is affected by expression, illumination, facial hair, makeup, and accessories. In our work, we present a novel local detector – Convolutional Experts Network (CEN) – that brings together the advantages of neural architectures and mixtures of experts in an end-to-end framework. We further propose a Convolutional Experts Constrained Local Model (CE-CLM) algorithm that uses CEN as local detectors. We demonstrate that our proposed CE-CLM algorithm outperforms competitive state-of-the-art baselines for facial landmark detection by a large margin on four publicly-available datasets. Our approach is especially accurate and robust on challenging profile images.*

## 1. Introduction

Facial landmark detection is an essential initial step for a number of research areas such as facial expression analysis, face 3D modeling, facial attribute analysis, multimodal sentiment analysis, emotion recognition and person identification [10, 22, 42, 30]. It is a well-researched problem with large amounts of annotated data and has seen a surge of interest in the past couple of years.

Until recently, one of the most popular methods for facial landmark detection was the family of Constrained Local Models (CLM) [10, 29]. They model the appearance of each

\* means equal contribution

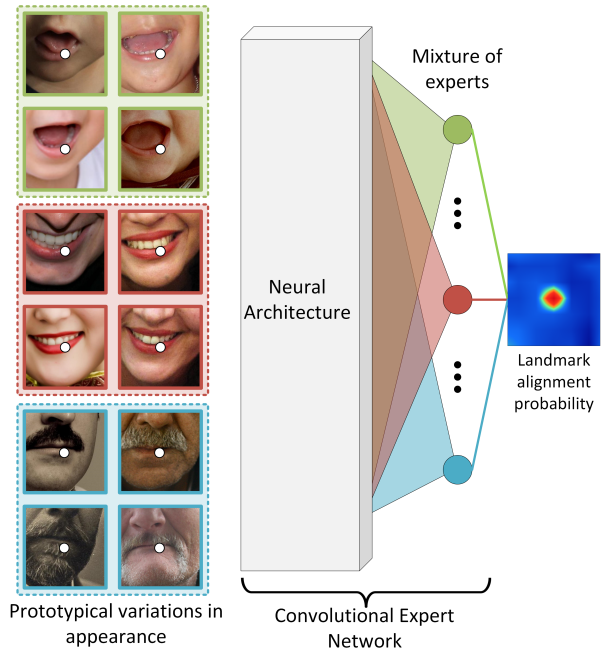


Figure 1: The appearance of a facial landmark naturally clusters around a set of appearance prototypes (such as facial hair, expressions, make-up etc.). In order to model such appearance variations effectively we introduce the Convolutional Experts Network (CEN) that brings together the advantages of neural architectures and mixtures of experts to model landmark alignment probability.

facial landmark individually using *local* detectors and use a shape model to perform *constrained* optimization. CLMs contain many benefits and extensions that many other approaches lack: 1) modeling the appearance of each landmark individually makes CLMs robust to occlusion [1, 29]; 2)

natural extension to a 3D shape model and multi-view local detectors allow CLMs to deal naturally with pose variations [29, 24] and landmark self-occlusions [3]; 3) the Expectation Maximization-based model leads to smoothness of tracking in videos [29]. This makes them a very appealing facial landmark detection and tracking method.

Despite these benefits, CLMs have been recently outperformed by various cascaded regression models [38, 48]. We believe that the relative under-performance of CLM based methods was due to the use of local detectors that are not able to model the complex variation of local landmark appearance as shown in Figure 1. A robust and accurate local detector should explicitly model these different *appearance prototypes* present in the same landmark.

This paper is an extended version of a CVPR-W submission which we introduce a novel local detector called Convolutional Experts Network (CEN) that brings together the advantages of neural architectures and mixtures of experts in an end-to-end framework [40]. CEN is able to learn a mixture of experts that capture different appearance prototypes without the need of explicit attribute labeling. To tackle facial landmark detection we present Convolutional Experts Constrained Local Model (CE-CLM), which is a CLM model that uses CEN as a local detector.

We evaluate both the benefits of our CEN local detector and CE-CLM facial landmark detection algorithm through an extensive set of experiments on four publicly-available datasets, 300-W [25], 300-VW [31], IJB-FL [15], and Menpo Challenge [44]. The latter two datasets include a large portion of profile face poses with extremely challenging conditions. Furthermore, we use the latter three for cross-dataset experiments.

The structure of this paper is as follows: we discuss related work in Section 2, CE-CLM is introduced in Section 3. In Section 4 we evaluate our CEN local detector and compare CE-CLM with other facial landmark detection approaches. We conclude the paper in Section 5.

## 2. Related Work

Facial landmark detection plays a crucial role in a number of research areas and applications such as facial attribute detection [18], facial expression analysis [22], emotion recognition and sentiment analysis [43, 41, 23, 39], and 3D facial reconstruction [14]. A full review of work in facial landmark detection is outside the scope of this paper and we refer the reader to recent reviews of the field [11, 37].

Modern facial landmark detection approaches can be split into two major categories: *model-based* and *regression-based*. *Model based* approaches often model both appearance and shape of facial landmarks explicitly with the latter constraining the search space and providing a form of regularization. *Regression-based* approaches on the other hand do not require an explicit shape model and landmark detec-

tion is directly performed on appearance. We provide a short overview of recent model and regression based methods.

**Model-Based** approaches find the best parameters of a face model that match the appearance of an image. A popular model-based method is the Constrained Local Model [10, 29] and its various extensions such as Constrained Local Neural Fields [2] and Discriminative Response Map Fitting [1] which use more advanced methods of computing local response maps and inferring the landmark locations.

Another noteworthy model-based approach is the mixture of trees model [50] which uses a tree based deformable parts model to jointly perform face detection, pose estimation and facial landmark detection. An extension of this approach is the Gauss-Newton Deformable Part Model [36] which jointly optimizes a part-based flexible appearance model along with a global shape using Gauss-Newton optimization. A more recently-proposed 3D Dense Face Alignment method [49] updates the parameters of a 3D Morphable Model [6] using a CNN and has shown good performance on facial landmark detection of profile faces.

**Regression-based** models predict the facial landmark locations directly from appearance. Majority of such approaches follow a cascaded regression framework, where the landmark detection is continually improved by applying a regressor on appearance given the current landmark estimate in explicit shape regression [7]. Cascaded regression approaches include the Stochastic Descent Method (SDM) [38] which uses SIFT [21] features with linear regression to compute the shape update and Coarse-to-Fine Shape Searching (CFSS) [48] which attempts to avoid a local optima by performing a coarse to fine shape search. Project out Cascaded regression (PO-CR) [35] is another cascaded regression example that updates the shape model parameters rather than predicting landmark locations directly.

Recent work has also used deep learning techniques for landmark detection. Coarse-to-Fine Auto-encoder Networks [45] use visual features extracted by an auto-encoder together with linear regression. Sun et al. [32] proposed a CNN based cascaded regression approach for sparse landmark detection. Similarly, Zhang et al. [47] proposed to use a CNN in multi-task learning framework to improve facial landmark performance by training a network to also learn facial attributes. Finally, Trigeorgis et al. [34] proposed Mnemonic Descent Method which uses a Recurrent Neural Network to perform cascaded regression on CNN based visual features extracted around landmark locations.

## 3. Convolutional Experts CLM

Convolutional Experts Constrained Local Model (CE-CLM) algorithm consists of two main parts: response map computation using Convolutional Experts Network and shape parameter update. During the first step, individual landmark alignment is estimated independently of the posi-

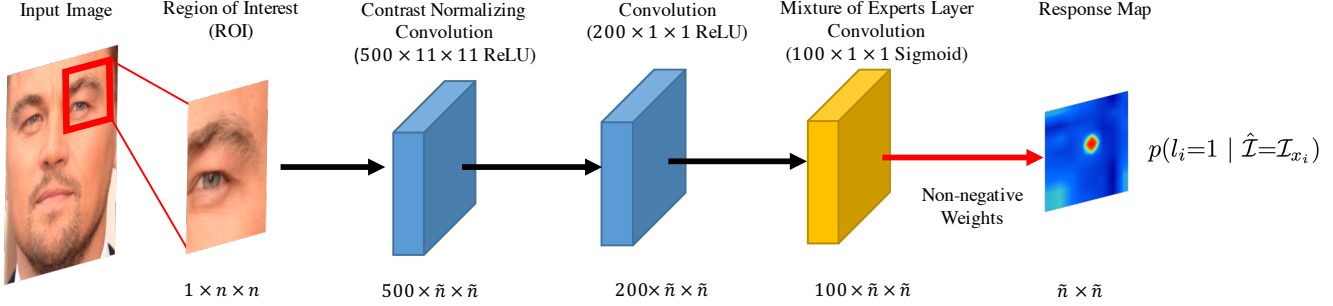


Figure 2: Overview of our Convolutional Experts Network model. Input image is given and based on the estimate of the landmark position a Region of Interest with size  $n \times n$  is extracted from it. This small region goes through a Contrast Normalizing Convolutional layer with kernel shape  $500 \times 11 \times 11$  which performs Z-score normalization before correlation operation that outputs a  $500 \times \tilde{n} \times \tilde{n}$  where  $\tilde{n} = n - 10$ . Afterwards, the response maps are input to a convolutional layer of  $200 \times 1 \times 1$  with ReLU units. Mixture of Expert Layer (ME-layer) learns an ensemble to capture ROI variations and uses a convolutional layer of  $100 \times 1 \times 1$  sigmoid probability decision kernels. The output response map is a non-negative and non-linear combination of neurons in ME-layer using a sigmoid activation.

tion of other landmarks. During the parameter update, the positions of all landmarks are updated jointly and penalized for misaligned landmarks and irregular shapes using a point distribution model. We optimize the following objective:

$$\mathbf{p}^* = \underset{\mathbf{p}}{\operatorname{argmin}} \left[ \sum_{i=1}^n -\mathcal{D}_i(x_i; \mathcal{I}) + \mathcal{R}(\mathbf{p}) \right] \quad (1)$$

above,  $\mathbf{p}^*$  is the optimal set of parameters controlling the position of landmarks (see Equation 3) with  $\mathbf{p}$  being the current estimate.  $\mathcal{D}_i$  is the alignment probability of landmark  $i$  in location  $x_i$  for input facial image  $\mathcal{I}$  (section 3.1) computed by CEN.  $\mathcal{R}$  is the regularization enforced by Point Distribution Model (Section 3.2). The optimization of Equation 1 is performed using Non-Uniform Regularized Landmark Mean Shift algorithm (Section 3.3).

### 3.1. Convolutional Experts Network

The first and most important step in CE-CLM algorithm is to compute a response map that helps to accurately localize individual landmarks by evaluating the landmark alignment probability at individual pixel locations. In our model this is done by CEN which takes a  $n \times n$  pixel region of interest (ROI) around the current estimate of a landmark position as input and outputs a response map evaluating landmark alignment probability at each pixel location. See Figure 2 for an illustration.

In CEN the ROI is first convolved with a contrast normalizing convolutional layer with shape  $500 \times 11 \times 11$  which performs Z-score normalization before calculating correlation between input and the kernel. The output response map is then convolved with a convolutional layer of  $200 \times 1 \times 1$  ReLU neurons.

The most important layer of CEN has the ability to model the final alignment probability through a mixture of experts

that can model different landmark appearance prototypes. This is achieved by using a special neural layer called Mixture of Expert Layer (ME-layer) which is a convolutional layer of  $100 \times 1 \times 1$  using sigmoid activation outputting individual experts vote on alignment probability (since sigmoid can be interpreted as probability). These response maps from individual experts are then combined using non-negative weights of the final layer followed by a sigmoid activation. This can be seen as a combination of experts leading to a final alignment probability. Our experiments show that ME-layer is crucial for performance of the proposed Convolutional Experts Network.

In simple terms, CEN is given an image ROI at iteration  $t$  of Equation 1 as input and outputs a probabilistic response map evaluating individual landmark alignment. Thus fitting the landmark  $i$  in position  $x_i$  follows the equation:

$$\pi_{x_i}^i = p(l_i = 1, \hat{\mathcal{I}} = \mathcal{I}_{x_i}) \quad (2)$$

$l_i$  is an indicator for landmark number  $i$  being aligned.  $\hat{\mathcal{I}}$  is the image ROI at location  $x_i$  for the image  $\mathcal{I}$ . The response maps  $\pi^i$  (of size  $\tilde{n} \times \tilde{n}$ ) are then used for minimizing Equation 1. The detailed network training procedure is presented in section 4.1 including chosen parameters for  $n$  at train and test time. Our experiments show that making CEN model deeper does not change the performance of the network. We study the effects of the ME-layer in section 4.1 using an ablation study.

### 3.2. Point Distribution Model

Point Distribution Models [9, 29] are used to both control the landmark locations and to regularize the shape in CE-CLM framework. Irregular shapes for final detected landmarks are penalized using the term  $\mathcal{R}(\mathbf{p})$  in the Equation 1. Landmark locations  $\mathbf{x}_i = [x_i, y_i]^T$  are parametrized

using  $\mathbf{p} = [s, \mathbf{t}, \mathbf{w}, \mathbf{q}]$  in the following 3D PDM Equation:

$$\mathbf{x}_i = s \cdot R_{2D} \cdot (\bar{\mathbf{x}}_i + \Phi_i \mathbf{q}) + \mathbf{t} \quad (3)$$

where  $\bar{\mathbf{x}}_i = [\bar{x}_i, \bar{y}_i, \bar{z}_i]^T$  is the mean value of the  $i^{\text{th}}$  landmark,  $\Phi_i$  a  $3 \times m$  principal component matrix, and  $\mathbf{q}$  an  $m$ -dimensional vector of non-rigid shape parameters;  $s$ ,  $R$  and  $\mathbf{t}$  are the rigid parameters:  $s$  is the scale,  $R$  is a  $3 \times 3$  rotation matrix defined by axis angles  $\mathbf{w} = [w_x, w_y, w_z]^T$  ( $R_{2D}$  are the first two rows of this matrix), and  $\mathbf{t} = [t_x, t_y]^T$  is the translation.

### 3.3. NU-RLMS

Equation 1 can be optimized using Non-Uniform Regularized Landmark Mean Shift (NU-RLMS) [2]. Given an initial CE-CLM parameter estimate  $\mathbf{p}$ , NU-RLMS iteratively finds an update parameter  $\Delta \mathbf{p}$  such that  $\mathbf{p}^* = \mathbf{p}_0 + \Delta \mathbf{p}$ , approaches the solution of Equation 1. NU-RLMS update finds the solution to the following problem:

$$\underset{\Delta \mathbf{p}}{\operatorname{argmin}} \left( \|\mathbf{p}_0 + \Delta \mathbf{p}\|_{\Lambda^{-1}}^2 + \|J\Delta \mathbf{p}_0 - \mathbf{v}\|_W^2 \right) \quad (4)$$

where  $J$  is the Jacobian of the landmark locations with respect to parameters  $\mathbf{p}$ .  $\Lambda^{-1}$  is the matrix of priors on  $\mathbf{p}$  with Gaussian prior  $\mathcal{N}(\mathbf{q}; 0, \Lambda)$  for non-rigid shape and uniform for shape parameters.  $W$  in Equation 4 is a weighting matrix for weighting mean shift vectors:  $W = w \cdot \operatorname{diag}(c_1; \dots; c_n; c_1; \dots; c_n)$  and  $c_i$  is the landmark detector accuracy calculated during model training based on correlation coefficient.  $\mathbf{v} = [v_i]$  is the mean-shift vector calculated using a Gaussian Kernel Density Estimator using response maps of CEN:

$$\mathbf{v}_i = \sum_{\mathbf{y}_i \in \Psi_i} \frac{\pi_{\mathbf{y}_i}^i \mathcal{N}(\mathbf{x}_i^c; \mathbf{y}_i, \rho \mathbf{I})}{\sum_{\mathbf{z}_i \in \Psi_i} \pi_{\mathbf{z}_i}^i \mathcal{N}(\mathbf{x}_i^c; \mathbf{z}_i, \rho \mathbf{I})} \quad (5)$$

$x_i^c$  is the current estimate for the landmark position and  $\rho$  is a hyper-parameter. This leads us to the update rule of NU-RLMS:

$$\Delta \mathbf{p} = -(J^T W J + r \Lambda_{-1})(r \Lambda_{-1} \mathbf{p} - J^T W \mathbf{v}) \quad (6)$$

## 4. Experiments

In our experiments we first evaluate the performance of Convolutional Experts Network and compare the performance with LNF [2] and SVR [29] local detectors (patch experts). We also evaluate the importance of the crucial ME-layer for CEN performance. Our final facial landmark detection experiments explore the use of our model in two settings: images and videos. All of our experiments were performed on challenging publicly available datasets and compared to a number of state-of-the-art baselines for within

Table 1: Comparison between CEN, LNF [2] and SVR [29] using square correlation  $r^2$  (higher is better) and RMSE (lower is better). To evaluate the necessity of the ME-layer we also compare to CEN (no ME-layer), a model with no non-negative constraint on the weights of ME-layer. Performance drop signals the crucial role of ME-layer.

| Detector          | $r^2$        | RMSE * $10^3$ |
|-------------------|--------------|---------------|
| SVR [29]          | 21.31        | 66.8          |
| LNF [2]           | 36.57        | 59.2          |
| CEN               | <b>64.22</b> | <b>37.9</b>   |
| CEN (no ME-layer) | 23.81        | 65.11         |

and cross-datasets. The CE-CLM and CEN training codes are available at 1) <https://github.com/A2Zadeh/CE-CLM>, 2) [multicomp.cs.cmu.edu/ceclm](http://multicomp.cs.cmu.edu/ceclm) and 3) as part of OpenFace [4] package <https://github.com/TadasBaltrusaitis/OpenFace>.

### 4.1. CEN Experiments

In this section we first describe training and inference methodology of the CEN local detector. We then compare the performance of CEN with LNF [2] and SVR [29] patch experts followed by an ablation study to investigate the crucial role of the ME-layer.

**Training Procedure:** for all of the experiments CEN was trained on LFPW and Helen training sets as well as Multi-PIE dataset. During training, if the landmark is located at the center of the  $11 \times 11$  convolutional region, then the probability for the landmark presence was high, otherwise low. A total of  $5 \times 10^5$  convolution regions were extracted for training set and  $6 \times 10^4$  were chosen for test set. We trained 28 sets of CENs per landmark: at seven orientations  $\pm 70^\circ, \pm 45^\circ, \pm 20^\circ, 0$  yaw; and four scales 17, 23, 30, and 60 pixel of interocular distance. To reduce the number of local detectors that needed to be trained we mirrored the local detectors at different yaw angles and used the same expert for left and right side of the face of the frontal view. The optimizer of CEN was Adam ([16]) with small learning rate of  $5 \times 10^{-4}$  and trained for 100 epochs with mini-batches of 512 (roughly 800,000 updates per landmark). For each landmark, scale and view a CEN local detectors has been trained. Training each CEN model takes 6 hours on a GeForce GTX Titan X but once trained inference can be quickly done and parallelized. We compare the performance improvement of CEN local detectors over LNF and SVR patch experts. Table 1 shows the average performance for each individual landmark. Since alignment probability inference is a regression task we use square correlation ( $r^2$ ) and RMSE between the ground truth validation set and local detector output as a measure of accuracy (higher is better for  $r^2$  and lower is better for RMSE). The train and test data for

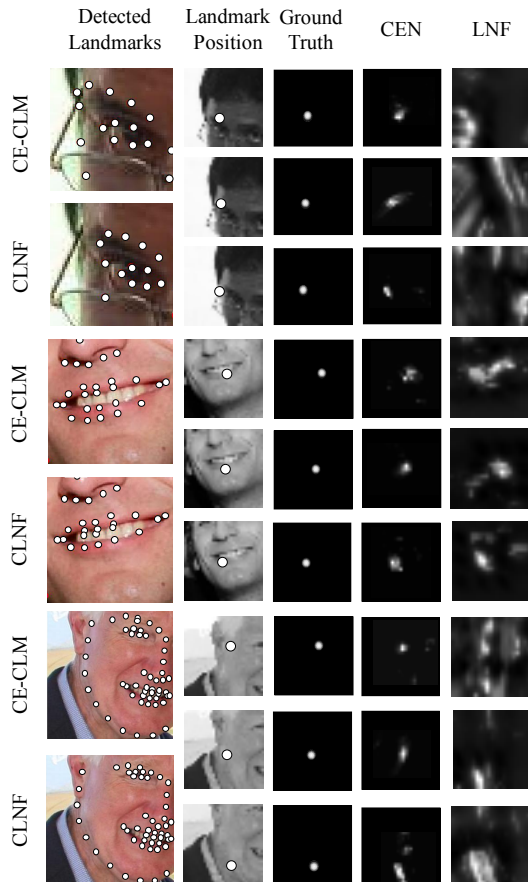


Figure 3: Comparison between response maps of CEN local detector and LNF patch experts across different landmarks. CEN shows better localization as the landmark probability is concentrated around the correct position of the landmark.

all the models are the same. On average CEN local detector performs 75.6% better than LNF and almost 200% better than SVR (calculated over  $r^2$ ), which shows a significant improvement. While this is an average, for certain landmarks, views and scales performance improvement is more than 100% over LNF. This is specifically the case for 17 pixel interocular distance scale since the CEN is able to model the location of landmark based on a bigger appearance of landmark neighborhood in the image (more context present in the image).

We also evaluate the importance of the ME-layer in the CEN model. Table 1 shows the difference between CEN and CEN (no ME-layer). We show that removing the non-negative constraint from the connection weights to final decision layer (essentially removing the model’s capability to learn mixture of experts) and retraining the network drops the performance significantly, almost to the level of SVR. This signals that ME-layer is a crucial and possibly the most

important part of CEN model capturing ranges of variation in texture, illumination and appearance in the input support region while removing it prevents the model from dealing with these variations.

In Figure 3 we visualize the improvement of CEN over LNF local detectors across different landmarks such as eyebrow region, lips and face outline. The ground truth response map is a normal distribution centered around the position of landmark. The output response map from CEN shows better certainty about the position of the landmark as its response map is more concentrated around the ground truth position. While LNF output is not showing such concentrated behavior. We therefore conclude that the major improvement from CEN comes from accurate local detection, and this directly transfers to improvement in landmark detection task.

## 4.2. CE-CLM Experiments

In this section we first describe the datasets used to train and evaluate our CE-CLM method. We then briefly discuss comparable state-of-the-art approaches for landmark detection. Finally we present the facial landmark detection results on images and videos.

### 4.2.1 Datasets

We evaluate our CE-CLM on four publicly available datasets: one within-dataset evaluation (300-W), and three cross-dataset evaluations (Menpo, IJB-FL, 300-VW). We believe that the cross-dataset evaluations present the strongest case of CE-CLM generalization when compared to the baselines. The datasets are described in more detail below.

**300-W** [25, 27] is a meta-dataset of four different facial landmark datasets: Annotated Faces in the Wild (AFW) [50], iBUG [26], and LFPW + Helen [5, 20] datasets. We used the full iBUG dataset and the test partitions of LFPW and HELEN. This led to 135, 224, and 330 images for testing respectively. They all contain uncontrolled images of faces *in the wild*: in indoor-outdoor environments, under varying illuminations, in presence of occlusions, under different poses, and from different quality cameras. We use the LFPW and HELEN test sets together with iBUG for model evaluation (as some baselines use AFW for training).

**Menpo** Benchmark Challenge [44] dataset is a very recent comprehensive multi-pose dataset for landmark detection in images displaying arbitrary poses. The training set consists of 8979 images, of which 2300 are profile images labeled with 39 landmark points; the rest of the images are labeled with 68 landmarks. The images for the dataset are mainly re-annotated images of the challenging AFLW [19] dataset.

**IJB-FL** [15] is a landmark-annotated subset of IJB-A [17] – a face recognition benchmark. It contains labels for 180 images (128 frontal and 52 profile faces). This is

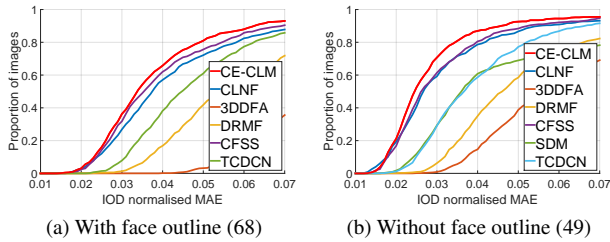


Figure 4: Cumulative error curves of IOD normalized facial landmark detection errors on the **300-W** test set – Helen, LFPW, and iBUG. CE-CLM performs better than all other approaches, especially in the difficult 68 landmark case. Best viewed in color.

a challenging subset containing images in non-frontal pose, with heavy occlusion and poor picture quality.

**300-VW**[31] test set contains 64 videos labeled for 68 facial landmarks for every frame. The test videos are categorized into three types: 1) laboratory and naturalistic well-lit conditions; 2) unconstrained conditions such as varied illumination, dark rooms and overexposed shots; 3) completely unconstrained conditions including illumination and occlusions such as occlusions by hand.

#### 4.2.2 Baselines

We compared our approach to a number of established baselines for the facial landmark detection task, including both cascaded regression and model based approaches. In all cases we use author provided implementations<sup>1</sup>, meaning we compare to the best available version of each baseline and using the same methodology.

**CFSS** [48] – Coarse to Fine Shape Search is a recent cascaded regression approach. It is the current state-of-the-art approach on the 300-W competition data [25, 8]. The model is trained on Helen and LFPW training sets and AFW.

**CLNF** is an extension of the Constrained Local Model that uses Continuous Conditional Neural Fields as patch experts [3]. The model was trained on LFPW and Helen training sets and CMU Multi-PIE [12].

**PO-CR** [35] – is a recent cascaded regression approach that updates the shape model parameters rather than predicting landmark locations directly in a projected-out space. The model was trained on LFPW and Helen training sets.

**DRMF** – Discriminative Response Map Fitting performs regression on patch expert response maps directly rather than using optimization over the parameter space. We use the

<sup>1</sup>We attempted to compare to the Mnemonic Descent Method [34], but were unable to compile the code provided by the authors due to the use of an older TensorFlow framework. As the authors do not provide results on publicly available datasets we were not able to compare our work to theirs.

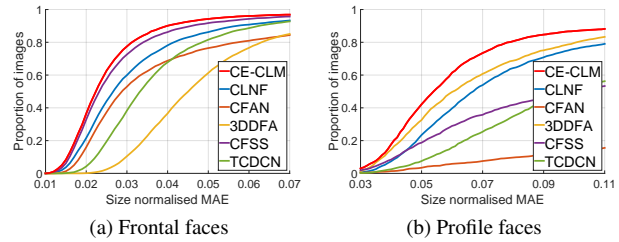


Figure 5: Results of our facial landmark detection on the **Menpo** dataset. CE-CLM outperforms all of the baselines in both the frontal and profile image case, with a very large margin in the latter. Best viewed in color.

implementation provided by the authors [1] that was trained on LFPW [5] and Multi-PIE [12] datasets.

**3DDFA** – 3D Dense Face Alignment [49] has shown state-of-the-art performance on facial landmark detection in profile images. The method uses the extended 300W-LP dataset [49] of synthesized large-pose face images from 300-W.

**CFAN** – Coarse-to-Fine Auto-encoder Network [45], uses cascaded regression on auto-encoder visual features that was trained on LFPW, HELEN and AFW.

**TCDCN** – Tasks-Constrained Deep Convolutional Network [47], is another deep learning approach for facial landmark detection that uses multi-task learning to improve landmark detection performance.

**SDM** – Supervised Descent Method is a very popular cascaded regression approach. We use implementation from the authors [38] that was trained on the Multi-PIE and LFW [13] datasets.

All of the above baselines were trained to detect either landmarks *without face outline* (49 or 51), or *with face outline* (66 or 68). For each comparison we used the biggest set of overlapping landmarks as all the approaches share the same subset of 49 feature points. For evaluating detections on profile images (present in IJB-FL and Menpo datasets), we use the subset of shared landmarks in ground truth images and detected ones. Since the annotations of Menpo profile faces differ slightly from the 68 landmark scheme we unify them by removing the two chin landmarks and using linear interpolation to follow the annotated curve to convert the 4 eyebrow landmarks to 5; and 10 face outline landmarks to 9. This still constitutes a fair comparison as none of the approaches (including ours) were trained on Menpo.

#### 4.2.3 Experimental setup

We use the same CEN multi-view and multi-scale local detectors as described in Section 4.1. Our PDM was trained on Multi-PIE and 300-W training datasets, using non-rigid

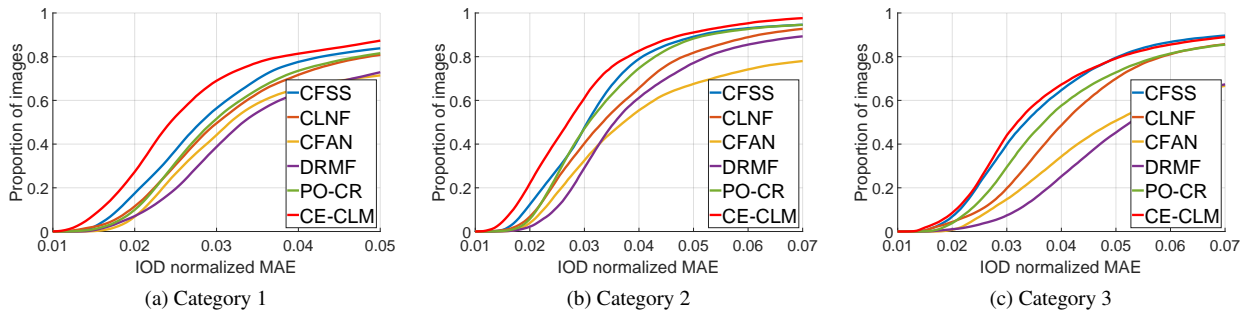


Figure 6: Results of our facial landmark detection and tracking on the **300-VW** dataset. CE-CLM outperforms all of the baselines in all of the three categories. We report results on 49 inner facial landmarks. Best viewed in color.

Table 2: The IOD normalized median error of landmark detection on the **300-W** dataset. We use the typical split: Comm. – Helen and LFPW, Diff. - iBUG.

| Approach   | With outline (68) |             | Without outline (49) |             |
|------------|-------------------|-------------|----------------------|-------------|
|            | Comm.             | Diff.       | Comm.                | Diff.       |
| CLNF [3]   | 3.47              | 6.37        | 2.51                 | 4.93        |
| SDM [38]   | -                 | -           | 3.31                 | 10.73       |
| CFAN [45]  | -                 | 8.38        | -                    | 6.99        |
| DRMF [1]   | 4.97              | 10.36       | 4.22                 | 8.64        |
| CFSS [48]  | 3.20              | 5.97        | 2.46                 | 4.49        |
| PO-CR [35] | -                 | -           | 2.67                 | <b>3.33</b> |
| TCDCN [47] | 4.11              | 6.87        | 3.32                 | 5.56        |
| 3DDFA [49] | 7.27              | 12.31       | 5.17                 | 8.34        |
| CE-CLM     | <b>3.14</b>       | <b>5.38</b> | <b>2.30</b>          | 3.89        |

Table 3: The size normalized median landmark error on the **Menpo** dataset. We present results for profile and frontal images separately. Our approach outperforms all of the baselines in both frontal and profile images.

| Approach   | With outline (68) |             | Without outline(49) |             |
|------------|-------------------|-------------|---------------------|-------------|
|            | Frontal           | Profile     | Frontal             | Profile     |
| CLNF [3]   | 2.66              | 6.68        | 2.10                | 4.43        |
| SDM [38]   | -                 | -           | 2.54                | 36.73       |
| CFAN [45]  | 2.87              | 25.33       | 2.34                | 28.1        |
| DRMF [1]   | -                 | -           | 3.44                | 36.1        |
| CFSS [48]  | 2.32              | 9.99        | 1.90                | 8.42        |
| PO-CR [35] | -                 | -           | 2.03                | 36.0        |
| TCDCN [47] | 3.32              | 9.82        | 2.81                | 8.69        |
| 3DDFA [49] | 4.51              | 6.02        | 3.59                | 5.47        |
| CE-CLM     | <b>2.23</b>       | <b>5.39</b> | <b>1.74</b>         | <b>3.32</b> |

structure from motion [33]. For model fitting we use a multi-scale approach, with a higher scale CEN used for each iteration. For each iteration we use a progressively smaller Region of Interest –  $\{25 \times 25, 23 \times 23, 21 \times 21, 21 \times 21\}$ .

Table 4: The size normalized median landmark error on the **IJB-FL** dataset. We present results for profile and frontal images separately. Our approach outperforms all of the baselines in both frontal and profile images.

| Approach   | With outline (68) |             | Without outline (49) |             |
|------------|-------------------|-------------|----------------------|-------------|
|            | Frontal           | Profile     | Frontal              | Profile     |
| CLNF [3]   | 4.39              | 7.73        | 3.82                 | 6.22        |
| SDM [38]   | -                 | -           | 3.93                 | 30.8        |
| CFAN [45]  | 4.89              | 20.26       | 4.37                 | 22.92       |
| DRMF [1]   | -                 | -           | 4.55                 | 25.52       |
| CFSS [48]  | 4.16              | 7.66        | 3.57                 | 6.79        |
| PO-CR [35] | -                 | -           | 3.73                 | 21.2        |
| TCDCN[47]  | 4.91              | 9.26        | 4.53                 | 9.09        |
| 3DDFA [49] | 5.90              | 8.14        | 4.85                 | 6.48        |
| CE-CLM     | <b>4.09</b>       | <b>6.31</b> | <b>3.47</b>          | <b>5.19</b> |

For NU-RLMS we set  $\sigma = 1.85$ ,  $r = 32$ ,  $w = 2.5$  based on grid-search on the training data. Given a bounding box, we initialized CE-CLM landmark locations at seven different orientations: frontal,  $\pm 30^\circ$  yaw, and  $\pm 30^\circ$  pitch, and  $\pm 30^\circ$  roll (we add four extra initializations  $\pm 55^\circ$ ,  $\pm 90^\circ$  yaw for Menpo and IJB-FL datasets due to large presence of profile faces). We perform early stopping and discarding of hypothesis evaluation if the converged maximum a posteriori score is above or below a threshold determined during validation. This early stopping improves the model speed by up to four times on average. During fitting we do not compute response maps of self-occluded landmarks and do not use them for parameter update.

For fairness of model comparison, the baselines and our model have been initialized using the same protocol. For 300-W dataset we initialized all of the approaches using the bounding boxes provided by the challenge organizers. For Menpo we initialized the approaches using a Multi-Task Convolutional Neural Network [46] face detector, which was able to detect faces in 96% of images. We performed an



Figure 7: Example images where our CE-CLM approach outperforms CFSS [48] and CLNF [2]. These are challenging images due to difficulties in pose, resolution and occlusion (glasses) but CE-CLM is able to align the 68 facial landmarks.

affine transformation of the bounding box to match that of bounding box around the 68 facial landmarks. For IJB-FL we initialized the approaches by generating a face bounding box by adding noise to the ground truth landmarks (based on the noise properties of the bounding boxes in 300-W dataset). For 300-VW we detected the face in every 30th frame of each video using a Multi-Task Convolutional Neural Network [46] face detector. When the face was not detected in the frame we used the closest frame with a successful detection instead. We performed a linear mapping from the detected bounding box to a tighter fit around all 68 landmarks (as done for Menpo dataset). Each baseline was initialized from the detection and allowed to track for 30 frames, either using previously detected landmarks or using the new bounding box.

#### 4.2.4 Landmark Detection Results

As common in such work we use commutative error curves of size normalized error per image to display landmark detection accuracy. We also report the size normalized median per image error. We report the median instead of the mean as the errors are not normally distributed and the mean is very susceptible to outliers. For datasets only containing close to frontal faces (300-W and 300-VW) we normalize the error by inter-ocular distance (IOD), for images containing profile faces where one of the eyes might not be visible we instead use the average of width and height of the face.

Results of landmark detection on the **300-W** dataset can be seen in Table 2 and Figure 4. Our approach outperforms all of the baselines in both the 68 and 49 point scenarios

(except for PO-CR in the 49 landmark case on the iBUG dataset). The improved accuracy of CE-CLM is especially apparent in the 68 landmark case which includes the face outline. This is a more difficult setup due to the ambiguity of face outline and which a lot of approaches (especially cascade regression based ones) do not tackle.

Results of landmark detection on the **IJB-FL** dataset can be seen in Table 4. CE-CLM model outperforms all of the baselines on this difficult task as well, with a large margin for profile faces.

Results of landmark detection on the **Menpo** dataset can be seen in Table 3 and Figure 5. CE-CLM model outperforms all of the baselines on this difficult task as well. The performance improvement is especially large on profile faces, which SDM, CFAN, DRMF, and PO-CR approaches are completely unable to handle. We also outperform the very recent 3DDFA model which was designed for large pose face fitting. As these results are on a cross-dataset evaluation, they demonstrate how well our method generalizes to unseen data and how well it performs on challenging profile faces (for example fits see Figure 7)

Results on landmark detection and tracking in videos on the **300-VW** dataset are displayed in Figure 6. CE-CLM consistently outperforms all of the baselines in all three categories with the biggest improvement in Category 1. Finally, our approach outperforms the recently proposed iCCR landmark tracking method that adapts to the particular person it tracks [28]. However, as it is a video approach this is not a fair comparison to our work and other baselines which treat each video frame independently. Note that our approach is consistently performing well for frontal and profile face

while other approaches perform well for frontal (CFSS, PO-CR) or profile (3DDFA). This is also true across different categories of 300-VW where other approaches performance varies across categories while CE-CLM consistently performs better than other approaches.

## 5. Conclusion

In this paper we introduced Convolutional Experts Constrained Local Model (CE-CLM), a new member of CLM family that uses a novel local detector called Convolutional Experts Network (CEN). Our proposed local detector is able to deal with varying appearance of landmarks by internally learning an ensemble of detectors, thus modeling landmark appearance prototypes. This is achieved through a Mixture of Expert Layer, which consists of decision neurons connected with non-negative weights to the final decision layer. In our experiments we show that this is a crucial part of CEN, which outperforms previously introduced local detectors of LNF and SVR by a big margin. Due to this better performance CE-CLM is able to perform better than state-of-the-art approaches on facial landmark detection and is both more accurate (Figure 4) and more robust, specifically in the case of profile faces (Figure 5). Figure 7 shows a visual comparison between CE-CLM, CFSS and CLNF landmark detection methods on a set challenging images. CE-CLM is able to accurately align landmarks even in extreme profile faces.

## References

- [1] A. Asthana, S. Zafeiriou, S. Cheng, and M. Pantic. Robust discriminative response map fitting with constrained local models. In *Proceedings of the IEEE Conference on Computer Vision and Pattern Recognition*, pages 3444–3451, 2013. 1, 2, 6, 7
- [2] T. Baltrušaitis, L.-P. Morency, and P. Robinson. Constrained local neural fields for robust facial landmark detection in the wild. In *IEEE International Conference on Computer Vision Workshops*, 2013. 2, 4, 8
- [3] T. Baltrušaitis, P. Robinson, and L.-P. Morency. Continuous conditional neural fields for structured regression. In *Computer Vision—ECCV 2014*, pages 593–608. Springer, 2014. 2, 6, 7
- [4] T. Baltrušaitis, P. Robinson, and L.-P. Morency. Openface: an open source facial behavior analysis toolkit. In *Applications of Computer Vision (WACV), 2016 IEEE Winter Conference on*, pages 1–10. IEEE, 2016. 4
- [5] P. N. Belhumeur, D. W. Jacobs, D. J. Kriegman, and N. Kumar. Localizing parts of faces using a consensus of exemplars. In *CVPR*, 2011. 5, 6
- [6] V. Blanz and T. Vetter. A Morphable Model For The Synthesis Of 3D Faces. In *SIGGRAPH*, pages 187–194, 1999. 2
- [7] X. Cao, Y. Wei, F. Wen, and J. Sun. Face alignment by Explicit Shape Regression. In *IEEE Conference on Computer Vision and Pattern Recognition*, pages 2887–2894. Ieee, jun 2012. 2
- [8] G. G. Chrysos, E. Antonakos, P. Snape, A. Asthana, and S. Zafeiriou. A Comprehensive Performance Evaluation of Deformable Face Tracking ”In-the-Wild”. 2016. 6
- [9] T. Cootes, G. Edwards, and C. Taylor. Active appearance models. *TPAMI*, 23(6):681–685, Jun 2001. 3
- [10] D. Cristinacce and T. Cootes. Feature detection and tracking with constrained local models. In *BMVC*, 2006. 1, 2
- [11] B. Czupryński and A. Strupczewski. *Active Media Technology: 10th International Conference, AMT 2014, Warsaw, Poland, August 11-14, 2014. Proceedings*, chapter High Accuracy Head Pose Tracking Survey, pages 407–420. Springer International Publishing, Cham, 2014. 2
- [12] R. Gross, I. Matthews, J. Cohn, T. Kanade, and S. Baker. Multi-pie. *IVC*, 28(5):807 – 813, 2010. 6
- [13] G. B. Huang, M. Ramesh, T. Berg, and E. Learned-Miller. *Labeled Faces in the Wild: A Database for Studying Face Recognition in Unconstrained Environments*. 2007. 6
- [14] L. A. Jeni, J. F. Cohn, and T. Kanade. Dense 3d face alignment from 2d video for real-time use. *Image and Vision Computing*, 2016. 2
- [15] K. KangGeon, T. Baltrušaitis, A. Zadeh, L.-P. Morency, and G. Medioni. Holistically constrained local model: Going beyond frontal poses for facial landmark detection. In *British Machine Vision Conference (BMVC)*, 2013. 2, 5
- [16] D. Kingma and J. Ba. Adam: A method for stochastic optimization <https://arxiv.org/abs/1412.6980>. 4
- [17] B. F. Klare, B. Klein, E. Taborsky, A. Blanton, J. Cheney, K. Allen, P. Grother, A. Mah, M. Burge, and A. K. Jain. Pushing the frontiers of unconstrained face detection and recognition: Iarpa janus benchmark a. In *Computer Vision and Pattern Recognition (CVPR), 2015 IEEE Conference on*, pages 1931–1939. IEEE, 2015. 5
- [18] N. Kumar, A. C. Berg, P. N. Belhumeur, and S. K. Nayar. Attribute and simile classifiers for face verification. In *Proceedings of the IEEE International Conference on Computer Vision*, pages 365–372, 2009. 2
- [19] M. Kstinger, P. Wohlhart, P. M. Roth, and H. Bischof. Annotated facial landmarks in the wild: A large-scale, real-world database for facial landmark localization. In *2011 IEEE International Conference on Computer Vision Workshops (ICCV Workshops)*, pages 2144–2151, Nov 2011. 5
- [20] V. Le, J. Brandt, Z. Lin, L. Bourdev, and T. S. Huang. Interactive facial feature localization. In *Computer Vision—ECCV 2012*, pages 679–692. Springer, 2012. 5
- [21] D. G. Lowe. Distinctive image features from scale invariant keypoints. *Int’l Journal of Computer Vision*, 60:91–11020042, 2004. 2
- [22] B. Martinez and M. Valstar. Advances, challenges, and opportunities in automatic facial expression recognition. In B. S. M. Kawulok, E. Celebi, editor, *Advances in Face Detection and Facial Image Analysis*, pages 63 – 100. Springer, 2016. 1, 2
- [23] S. Poria, E. Cambria, D. Hazarika, N. Mazumder, A. Zadeh, and L.-P. Morency. Context-dependent sentiment analysis in user-generated videos. In *Association for Computational Linguistics*, 2017. 2

- [24] G. Rajamanoharan and T. F. Cootes. Multi-view constrained local models for large head angle facial tracking. In *The IEEE International Conference on Computer Vision (ICCV) Workshops*, December 2015. 2
- [25] C. Sagonas, G. Tzimiropoulos, S. Zafeiriou, and M. Pantic. 300 faces in-the-wild challenge: The first facial landmark localization challenge. In *Proceedings of the IEEE International Conference on Computer Vision Workshops*, pages 397–403, 2013. 2, 5, 6
- [26] C. Sagonas, G. Tzimiropoulos, S. Zafeiriou, and M. Pantic. 300 faces in-the-wild challenge: The first facial landmark localization challenge. In *ICCV*, 2013. 5
- [27] C. Sagonas, G. Tzimiropoulos, S. Zafeiriou, and M. Pantic. A semi-automatic methodology for facial landmark annotation. In *Proceedings of the IEEE Conference on Computer Vision and Pattern Recognition Workshops (CVPR-W), Workshop on Analysis and Modeling of Faces and Gestures*, 2013. 5
- [28] E. Sánchez-Lozano, B. Martinez, G. Tzimiropoulos, and M. Valstar. Cascaded Continuous Regression for Real-time Incremental Face Tracking. In *ECCV*, 2016. 8
- [29] J. Saragih, S. Lucey, and J. Cohn. Deformable Model Fitting by Regularized Landmark Mean-Shift. *IJCV*, 2011. 1, 2, 3, 4
- [30] E. Sariyanidi, H. Gunes, and A. Cavallaro. Automatic analysis of facial affect: A survey of registration, representation and recognition. *IEEE TPAMI*, 2014. 1
- [31] J. Shen, S. Zafeiriou, G. G. Chrysos, J. Kossaifi, G. Tzimiropoulos, and M. Pantic. The First Facial Landmark Tracking in-the-Wild Challenge: Benchmark and Results. *2015 IEEE International Conference on Computer Vision Workshop (ICCVW)*, 2015. 2, 6
- [32] Y. Sun, X. Wang, and X. Tang. Deep convolutional network cascade for facial point detection. *Proceedings of the IEEE Computer Society Conference on Computer Vision and Pattern Recognition*, pages 3476–3483, 2013. 2
- [33] L. Torresani, A. Hertzmann, and C. Bregler. Nonrigid structure-from-motion: Estimating shape and motion with hierarchical priors. *TPAMI*, 30(5):878–892, may 2008. 6
- [34] G. Trigeorgis, P. Snape, M. A. Nicolaou, E. Antonakos, and S. Zafeiriou. Mnemonic Descent Method: A recurrent process applied for end-to-end face alignment. In *CVPR*, 2016. 2, 6
- [35] G. Tzimiropoulos. Project-Out Cascaded Regression with an application to Face Alignment. In *CVPR*, 2015. 2, 6, 7
- [36] G. Tzimiropoulos and M. Pantic. Gauss-newton deformable part models for face alignment in-the-wild. In *Proceedings of the IEEE Conference on Computer Vision and Pattern Recognition*, pages 1851–1858, 2014. 2
- [37] N. Wang, X. Gao, D. Tao, and X. Li. Facial Feature Point Detection: A Comprehensive Survey. page 32, 2014. 2
- [38] X. Xiong and F. Torre. Supervised descent method and its applications to face alignment. In *Proceedings of the IEEE conference on computer vision and pattern recognition*, pages 532–539, 2013. 2, 6, 7
- [39] A. Zadeh. Micro-opinion sentiment intensity analysis and summarization in online videos. In *Proceedings of the 2015 ACM on International Conference on Multimodal Interaction*, pages 587–591. ACM, 2015. 2
- [40] A. Zadeh, T. Baltrušaitis, and L.-P. Morency. Convolutional experts constrained local model for facial landmark detection. In *Computer Vision and Pattern Recognition Workshop (CVPRW)*. IEEE, 2017. 2
- [41] A. Zadeh, M. Chen, S. Poria, E. Cambria, and L.-P. Morency. Tensor fusion network for multimodal sentiment analysis. In *Empirical Methods in NLP*, 2017. 2
- [42] A. Zadeh, R. Zellers, E. Pincus, and L.-P. Morency. Mosi: Multimodal corpus of sentiment intensity and subjectivity analysis in online opinion videos. *arXiv preprint arXiv:1606.06259*, 2016. 1
- [43] A. Zadeh, R. Zellers, E. Pincus, and L.-P. Morency. Multi-modal Sentiment Intensity Analysis in Videos: Facial Gestures and Verbal Messages. *2016 IEEE Intelligent Systems*, 2016. 2
- [44] S. Zafeiriou. The menpo facial landmark localisation challenge. In *Computer Vision and Pattern Recognition Workshops (CVPRW)*, 2017. 2, 5
- [45] J. Zhang, S. Shan, M. Kan, and X. Chen. Coarse-to-fine auto-encoder networks (cfan) for real-time face alignment. In *ECCV*. Springer, 2014. 2, 6, 7
- [46] K. Zhang, Z. Zhang, Z. Li, and Y. Qiao. Joint face detection and alignment using multitask cascaded convolutional networks. *IEEE Signal Processing Letters*, 23(10):1499–1503, Oct 2016. 7, 8
- [47] Z. Zhang, P. Luo, C.-C. Loy, and X. Tang. Facial Landmark Detection by Deep Multi-task Learning. In *ECCV*, 2014. 2, 6, 7
- [48] S. Zhu, C. Li, C. C. Loy, and X. Tang. Face Alignment by Coarse-to-Fine Shape Searching. In *CVPR*, 2015. 2, 6, 7, 8
- [49] X. Zhu, Z. Lei, X. Liu, H. Shi, and S. Z. Li. Face Alignment Across Large Poses: A 3D Solution. In *CVPR*, 2016. 2, 6, 7
- [50] X. Zhu and D. Ramanan. Face detection, pose estimation, and landmark localization in the wild. In *Computer Vision and Pattern Recognition (CVPR), 2012 IEEE Conference on*, pages 2879–2886. IEEE, 2012. 2, 5